Research Article

Feng Yu, Xing Chen, Yuan Fang*, Yue Cao, Shuangshuang Bu, and Shijiang Zhang

Study on the basic properties of iron tailings powder-desulfurization ash mine filling cementitious material

https://doi.org/10.1515/secm-2024-0024
received February 27, 2024; accepted May 21, 2024

Abstract: To realize the recycling of iron tailings powder (IP) and desulfurization ash (DA) and reduce the high preparation cost of mine filling cementitious materials (MCs), this article adopts sodium carbonate (SC) as an activator to prepare iron tailings powder-desulfurization ash mine filling cementitious materials (IDMC). The effects of IP content, DA content, SC content, and mirabilite content on the mechanical properties and setting time are experimentally investigated. The micromorphology and phase compositions of the hydration products of IDMC are analyzed and characterized by scanning electron microscopy and X-ray diffraction. The results show that the initial setting time of the IDMC is reduced by 0.87 and 21.83% when the mirabilite content is increased from 0 to 1% and 2%, respectively, and the compressive and flexural strengths of the IDMC are increased by 24.01 and 86.25% when the IP content is increased from 0 to 20%, respectively. The IP not only participates in the hydration reaction but also plays an aggregate filling effect, significantly improving the mechanical properties of the IDMC. The pozzolanic effect is gradually enhanced with the increase of the DA content, and the hydration degree of the IDMC increases. The SC as an activator can moderately reduce the shrinkage rate of the IDMC. Based on the multi-index optimization analysis, the optimal mix proportion of the IDMC is obtained, which provides an effective reference for the preparation of the novel MC.

Keywords: mine filling, cementitious material, iron tailings powder, desulfurization ash, setting time, mechanical property

Abbreviations

IP	Iron tailings powder
DA	Desulfurization ash
MC	Mine filling cementitious materials
SC	Sodium carbonate
IDMC	Iron tailings powder-desulfurization ash mine filling cementitious materials
SEM	Scanning electron microscopy
XRD	X-ray diffraction
C–S–H	Calcium silicate hydrated
AFt	Ettringite
C_3S	Tricalcium silicate
C_3A	Tricalcium aluminate

1 Introduction

Iron tailings are solid waste produced by mineral processing. Continuous exploitation of mineral resources has led to the accumulation of a large amount of iron tailings, and the current global available iron tailings output is approximately 2.5 billion tons [1]. Waste iron tailings occupy a lot of land, pollute the surrounding ecological environment, and require expensive processing and maintenance costs. Similarly, another type of industrial solid waste, desulfurization ash (DA), which also has a massive accumulation, is produced in dry or dry flue gas desulphurization of coal-fired boilers [2,3]. Due to the significant amount of unstable calcium sulfite in its composition, its application in engineering fields is greatly limited [4]. Therefore, how to reasonably and effectively use these two solid waste resources has become a widespread concern and an urgent problem to be solved.

* **Corresponding author: Yuan Fang**, School of Civil Engineering and Architecture, Anhui University of Technology, Ma'anshan, 243032, China, e-mail: fyuan86@126.com
Feng Yu: School of Civil Engineering and Architecture, Anhui University of Technology, Ma'anshan, 243032, China; Wuhu Technology and Innovation Research Institute, Anhui University of Technology, Wuhu, 241002, China
Xing Chen, **Yue Cao**, **Shuangshuang Bu**, **Shijiang Zhang:** School of Civil Engineering and Architecture, Anhui University of Technology, Ma'anshan, 243032, China

Iron tailing sand has a similar physical morphology and mechanical properties to natural sand. The existing studies confirmed that it was feasible to substitute iron tailing sand for natural sand as fine aggregate in mortar and concrete [5–13]. Meanwhile, iron tailings powder (IP) with a small particle size could be used to prepare cementitious materials [14–17]. Deng *et al.* [18] mixed ultra-fine tailings and cement at a ratio of 1:3–1:8 to prepare underground filling cementing materials that met mining technique requirements. To protect the mining environment and maximize the recovery of waste tailings, Lu *et al.* [19] backfilled abandoned tailings as cement slurry in underground mines and open pit mines. The solid content of the cemented paste backfill was 72%, and the cement-tailings ratios were 1:8, 1:10, and 1:20. Shirengou Iron Mine has achieved 100% abandoned tailings recovery rate by adopting the new procedure. Chu *et al.* [20] prepared mine filling cementitious materials (MC) by mixing river sediment, IP, and calcium carbide slag. The results showed that the slump value was 160 mm and the 7 days unconfined compressive strength was 2.8 MPa, which met the requirements of mine filling. These existing studies confirmed the feasibility of preparing MC with iron tailings; however, the defects of the prepared MC with a large shrinkage rate and high preparation cost greatly limited its wide application and development in engineering [21,22].

Under the action of activator, the DA underwent hydration reaction to generate calcium silicate hydrated (C–S–H) and ettringite (AFt), which could effectively improve the early strength of the cementitious materials and reduce the water absorption and porosity of the materials [23–27]. Li *et al.* [28] modified the DA by the chemical activation method, and the particle size distribution of the modified DA was effectively optimized, and its water requirement was significantly reduced. The 28 days strength of mortar was equal to that of Portland cement when the content of the DA was not less than 10%. Wang *et al.* [29] used the activator to activate the pozzolanic activity of the DA to prepare DA mortar and demonstrated that the 7 and 28 days compressive strengths of cementitious materials could reach 20 and 22.3 MPa, respectively. These investigations confirmed that the DA cementitious materials prepared with appropriate activators could obtain favorable mechanical properties. However, the use of alkaline activator would increase the shrinkage of the cementitious material [30].

In recent years, scholars prepared cementitious materials by reasonably mixing discarded IP and DA, carried out the corresponding research on mechanical properties [31–33], and found that IP and DA could be used as cementing components and reasonable mixing could improve the mechanical properties of cementitious materials. However, these limited investigations did not consider the effects of activators but only produced cementing materials by partially substituting cement with mixed solid waste materials. In view of the positive effect of the activator, Frasson and Rocha [34] studied the performance of sodium carbonate (SC)-activated slag materials and demonstrated that SC as an activator could efficiently improve the mechanical properties and moderately reduce the shrinkage rate of cementitious material.

To realize the reuse of industrial waste recourse and reduce the preparation cost of the MC, the IDMC was prepared with SC as an activator. The effects of IP content, DA content, SC content, and mirabilite content on the mechanical properties and setting time of the IDMC were experimentally analyzed. The micro morphology and phase compositions of hydration products were investigated. This study attempts to address the recycling and utilization of the IP and DA solid wastes. The cementitious properties and early strength of IP mortar can be improved by the incorporation of the DA, and the increased activator will accelerate the early hydration reaction rate of the cementitious materials, improve the early mechanical strength, and simultaneously reduce the preparation costs, which provides a new method for the preparation of MC. An overview of the different sections of this study is shown in Figure 1.

2 Experimental scheme

2.1 Raw materials

Raw materials include IP, DA, slag powder, SC, mirabilite, and water, as depicted in Figure 2. The chemical compositions of IP, DA, and slag powder are listed in Tables 1–3, respectively. For IP and DA, the high proportions of SiO_2 and Al_2O_3 in the chemical composition indicate the cementitious activity. The chemical composition of slag powder is mainly SiO_2, Al_2O_3, CaO, and MgO, which provides the feasibility as cementitious components. Table 4 lists the morphology and performance indexes of raw materials.

2.2 Experimental design

To analyze the effects of the IP content, DA content, SC content, and mirabilite content on the mechanical properties and setting time of the IDMC, an orthogonal experiment with four factors and three levels was designed, as shown in Table 5. The IP content, DA content, SC content,

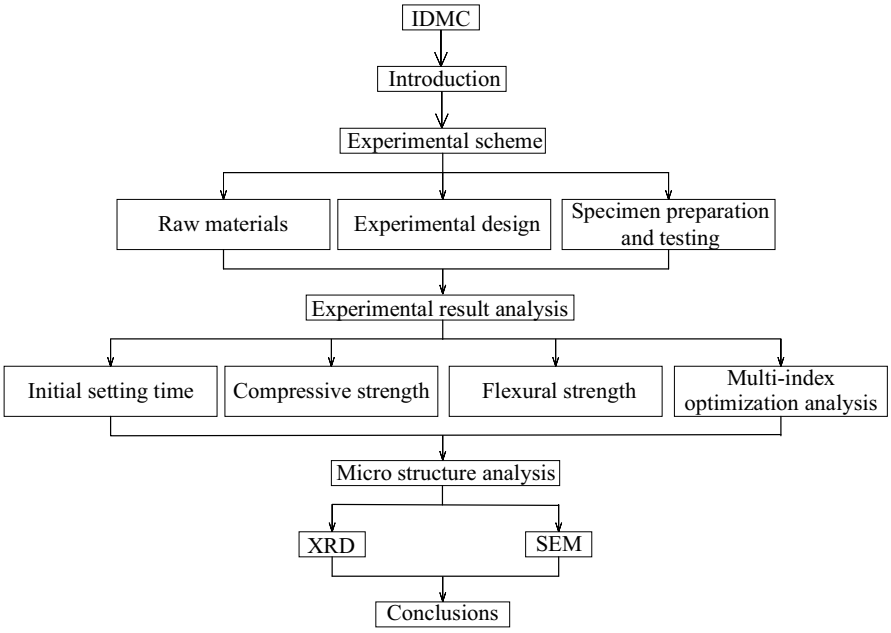

Figure 1: An overview of the different sections.

and mirabilite content were factors A, B, C, and D, respectively. The K1, K2, and K3 of factor A were 0, 20, and 40%, respectively. The K1, K2, and K3 of factor B were 0, 5, and 10%, respectively. The K1, K2, and K3 of factor C were 0, 1, and 2%, respectively. The K1, K2, and K3 of factor D were 0, 1, and 2%, respectively.

2.3 Specimen preparation and testing

First, the IP, DA, and slag powder were poured into a mixer and mixed for 1 min at low speed to make the powder uniformly compounded. Then, the appropriate amount of water was poured and mixed at low speed for 2 min. After

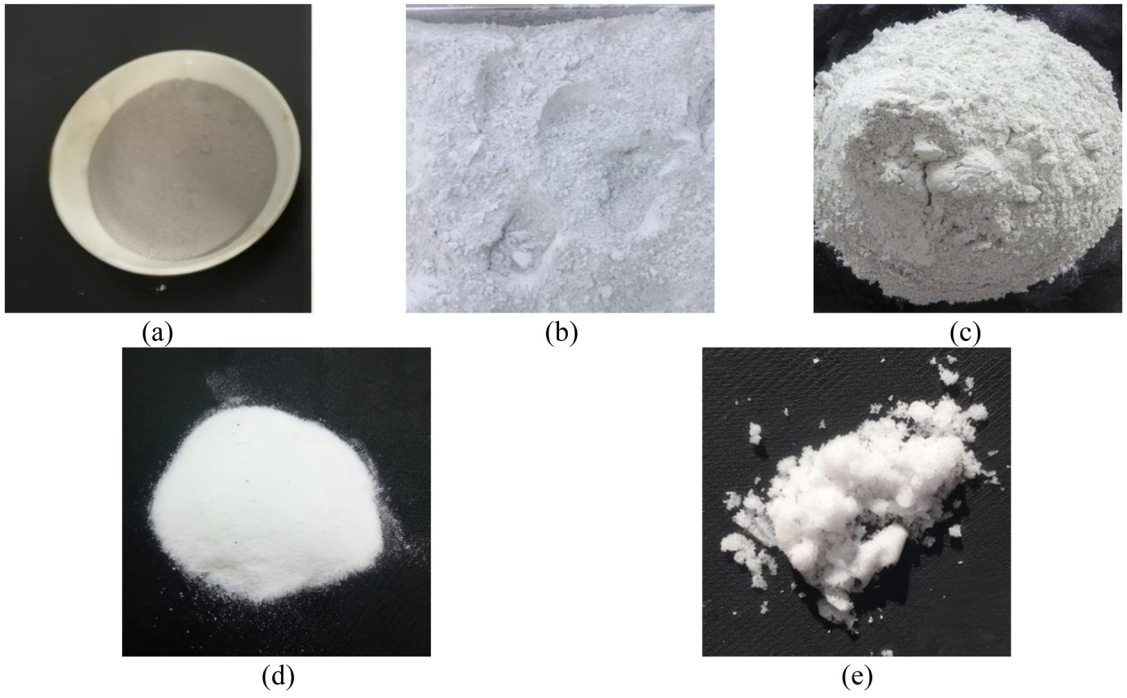

Figure 2: Raw materials of the IDMC: (a) IP, (b) DA, (c) slag powder, (d) SC, and (e) mirabilite.

Table 1: The chemical compositions of the IP (%)

SiO_2	Al_2O_3	Fe_2O_3	CaO	MgO	P_2O_5	K_2O	Na_2O	MnO	TiO_2
61.63	16.22	11.09	6.35	2.86	0.62	0.32	0.29	0.28	0.17

Table 2: The chemical compositions of the DA (%)

SiO_2	Al_2O_3	CaO	SO_3	MgO	Fe_2O_3	Na_2O	Cl	TiO_2	I
36.23	23.36	17.56	10.24	6.86	1.62	1.32	1.29	0.98	0.54

Table 3: The chemical compositions of slag powder (%)

CaO	SiO_2	Al_2O_3	MgO	S	Na_2O	TiO_2	K_2O	Fe_2O_3	MnO
38.06	35.06	17.12	6.20	1.33	1.32	1.07	0.93	0.32	0.30

the slurry was stable and uniform, SC, mirabilite, and the remaining water were added and stirred at high speed for 3 min. Finally, the slurry was poured into a triple steel mold with a size of 40 mm × 40 mm × 160 mm. After marking, the samples were stored in the maintenance room for standard curing at 20 ± 3°C and a relative humidity of not less than 90%. The preparation process of the IDMC is shown in Figure 3.

The initial setting time of the IDMC was tested following the Chinese standard "Test methods for water requirement of normal consistency, setting time and soundness of the Portland cement" GB/T1346-2011 [35]. The 28 days compressive and flexural tests were conducted according to the Chinese standard GB/T17671-2021 [36]. YAW-200B testing machine and DKZ-5000 testing machine were used to measure the compressive strength and flexural strength of the samples, respectively, as shown in Figure 4. According to the characteristics of the sample material, the flexural testing machine was uniformly loaded at a loading rate of 50 ± 10 N/s until the samples were broken. The compression testing machine was uniformly loaded at a loading rate of 1.5 ± 0.125 MPa/s until the samples failed. The load–displacement curves of the samples for compressive and flexural tests are shown in Figures 5 and 6, respectively. To investigate the hydration mechanism of the IDMC, the D8ADVANCE X-ray diffraction (XRD) and SU8220 scanning electron microscopy (SEM) were employed to analyze the phase composition and micromorphology of the IDMC at 28 days curing. Table 5 lists the results of initial setting time, 28 days compressive strength, and flexural strength of the samples.

Table 4: Main technical indexes of material

Material	Main technical feature
IP	Appearance: gray powder
	Density: 2.73 g/cm^3
	Bulk density: 1,500 kg/m^3
	Specific surface area: 371–466 m^2/g
	Moisture content: 0.91
	Particle size: 28.0–164.5 μm
	Fineness modulus: 2.178
DA	Appearance: light brown powder
	Density: 2.76 g/cm^3
	Bulk density: 996 kg/m^3
	Specific surface area: 536 m^2/g
	Moisture content: 0.89
	Particle size: 1.2–4.4 μm
Slag powder	Appearance: white powder
	Density: 2.65 g/cm^3
	Bulk density: 982 kg/m^3
	Specific surface area: 345–456 m^2/g
	Moisture content: 0.77
	Particle size: 21.0–60 μm
SC	Appearance: white powder
	Density: 2.52 g/cm^3
	Specific surface area: 268 m^2/g
	Na_2CO_3 content: 99.5%
	Melting point: 318°C
	Water-solubility: 51 g (20°C)
Mirabilite	Appearance: white crystalline powder
	Density: 2.68 g/cm^3
	Specific surface area: 997 m^2/g
	$Na_2SO_4{\cdot}10H_2O$ content: 98%
	Melting point: 884°C
	Water-solubility: 185 g (20°C)

Table 5: Orthogonal experiment ($L^9(4^3)$)

Group	A	B	C	D	Slag powder (%)	Initial setting time (min)	28 days compressive strength (MPa)	28 days flexural strength (MPa)
1	0	0	0	0	100	335	3.81	0.68
2	0	5	1	1	93	324	4.28	0.9
3	0	10	2	2	86	256	4.04	0.83
4	20	0	1	2	77	252	5.17	1.57
5	20	5	2	0	73	334	4.85	1.28
6	20	10	0	1	69	346	5.01	1.61
7	40	0	2	1	57	361	3.04	0.61
8	40	5	0	2	53	305	3.23	0.77
9	40	10	1	0	49	371	3.42	0.84

3 Experimental result analysis

3.1 Initial setting time

The impact of various factors on the initial setting time is analyzed in this section. Figure 7 presents the initial setting time of the IDMC at different influencing levels. Figure 8 analyzes the range and variance of the IDMC initial setting time. Clearly, the influence degree of each factor on initial setting time is as follows: D > A > C > B.

Mirabilite content D exerts the greatest influence on the initial setting time. The initial setting time of the IDMC decreased as the mirabilite content increased. This is because the dissolution rate of the mirabilite is faster,

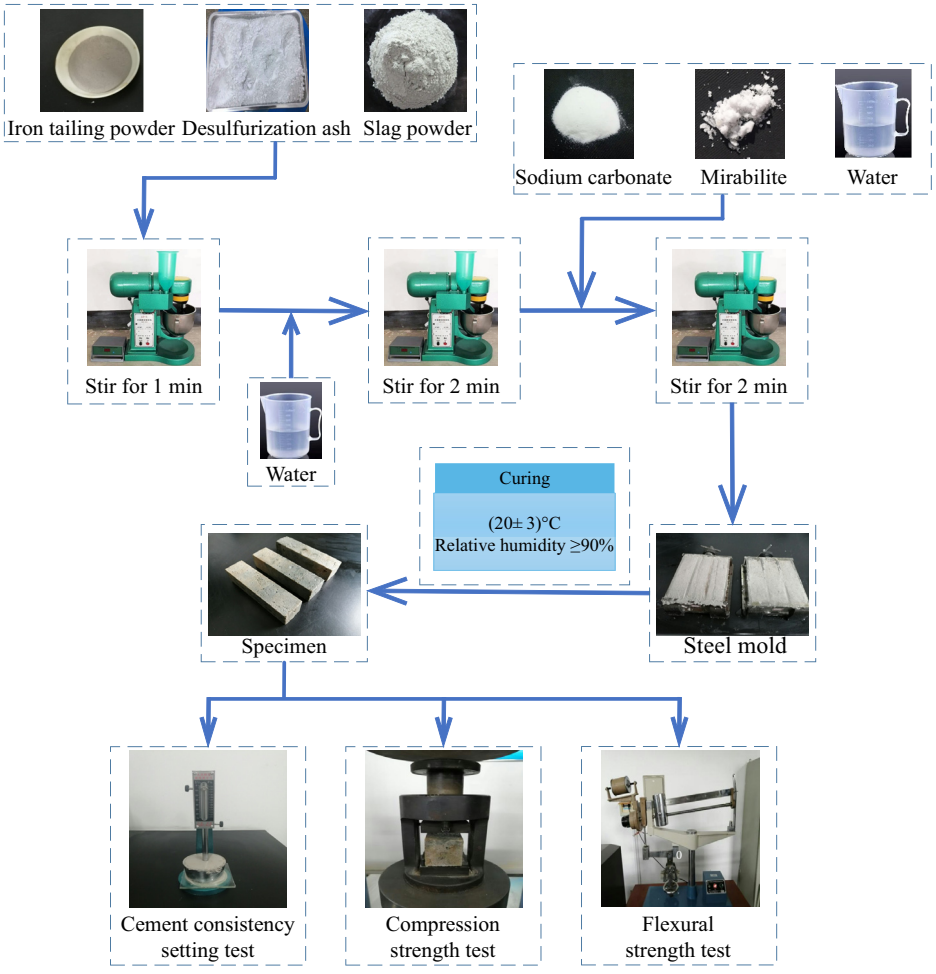

Figure 3: Preparation flowchart of the IDMC.

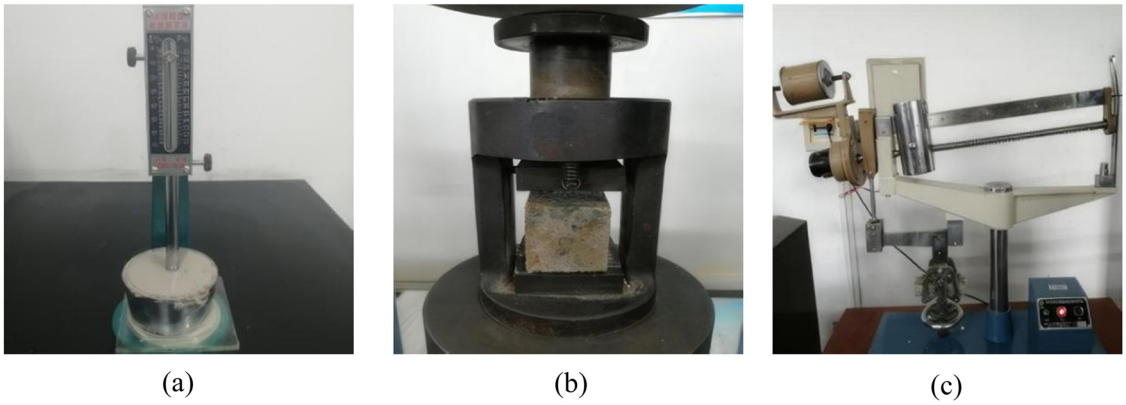

Figure 4: Mechanical properties testing apparatus: (a) cement consistency setting tester, (b) compression testing machine, and (c) flexural strength tester.

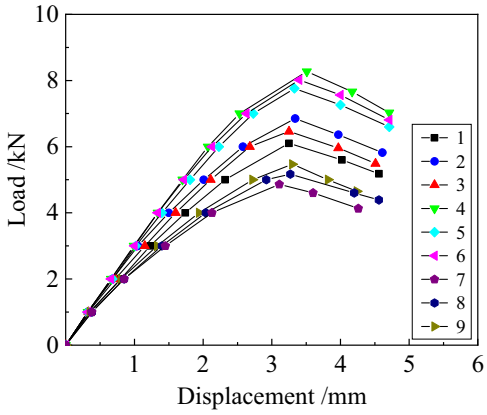

Figure 5: Load–displacement curves of the samples for compression tests.

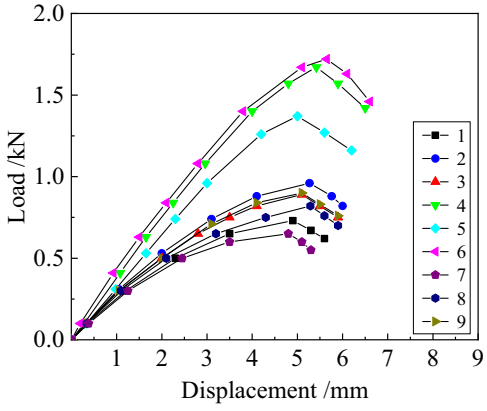

Figure 6: Load–displacement curves of the samples for flexural tests.

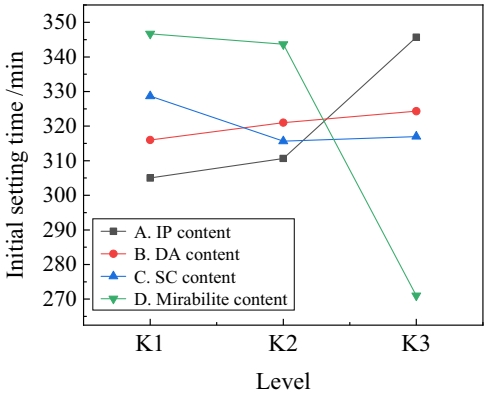

Figure 7: The initial setting time at different levels.

and the depolymerized Ca^{2+} in the IDMC reacts with SO_4^{2-} in mirabilite to produce $CaSO_4$ precipitation and a large amount of Na^+. The vitreous depolymerization of IP, slag powder, and DA can be accelerated by forming an alkaline environmental solution. Meanwhile, the hydration of tricalcium silicate (C_3S) and tricalcium aluminate (C_3A) can also be accelerated, and some hydration products react with $NaSO_4$ in the mirabilite to generate AFt, which further promotes the hydration reaction of the IDMC, resulting in a shorter initial setting time of the IDMC. Comparatively, the A, B, and C have a little impact on the initial setting time of the IDMC. When the content of DA, SC, and IP is 0, 1, and 20%, respectively, the initial setting time of the IDMC is the shortest. To reduce the initial setting time of the IDMC and to improve its early strength, the mixing proportion of the IDMC with the shortest initial setting time is $A_{K2}B_{K1}C_{K2}D_{K3}$.

3.2 Compressive strength

Figure 9 illustrates the 28 days compressive strength of the IDMC at different influencing levels. Figure 10 analyzes the variance and range of the 28 days compressive strength of the IDMC. As can be seen from the figure, the influences of

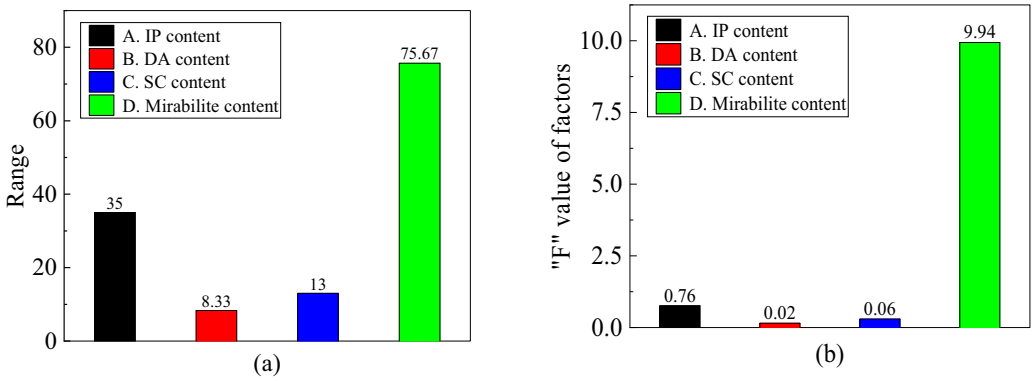

Figure 8: Range and variance analysis of initial setting time: (a) range analysis and (b) variance anlysis.

various factors on 28 days compressive strength are different from those of the aforementioned setting time, as follows: A > C > B > D. The IP content shows the greatest influence on the 28 days compressive strength of the IDMC. Apparently, with the increase of the IP content, the 28 days compressive strength of the IDMC increases and then decreases. When the content of IP is 20%, the 28 days compressive strength reaches the maximum. The IP plays the role of aggregate filling, reducing porosity, and improving compressive strength. However, the cementitious activity of IP is much smaller than that of slag micro powder. With the increase of the IP content, the C–S–H gels generated by the hydration of slag powder are reduced. The IP particles cannot be completely wrapped by C–S–H gels, and the internal compactness of samples reduces, thereby decreasing 28 days compressive strength. However, the 28 days compressive strength of the IDMC is almost not affected by the B, C, and D. When the contents of DA, SC, and mirabilite is 10, 1, and 2%, respectively, the 28 days compressive strength is the largest. The optimum mixing ratio for the samples to achieve maximum compressive strength is $A_{K2}B_{K3}C_{K2}D_{K3}$.

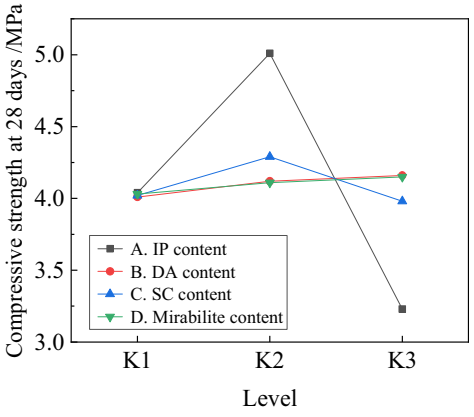

Figure 9: The 28 days compressive strength at different levels.

3.3 Flexural strength

The 28 days flexural strength of the IDMC at different influencing levels is shown in Figure 11. The range and variance analysis of the 28 days flexural strength of the IDMC are

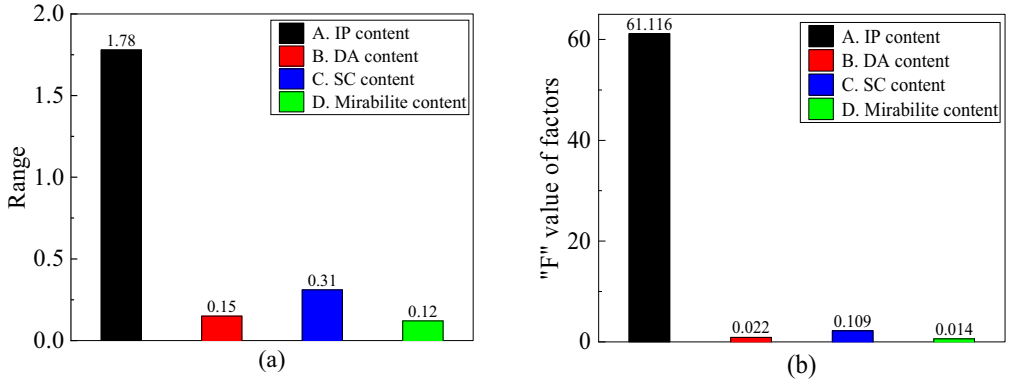

Figure 10: Range and variance analysis of 28 days compressive strength: (a) range analysis and (b) variance anlysis.

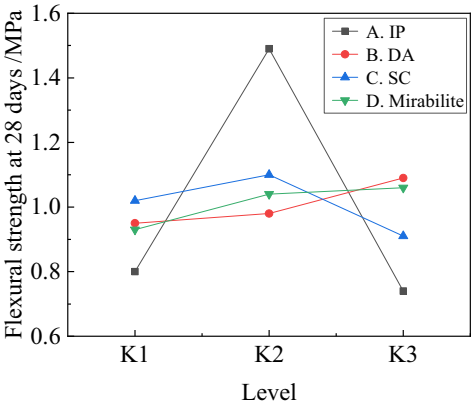

Figure 11: The 28 days flexural strength at different levels.

shown in Figure 12. The influence degree of various factors on the 28 days flexural strength of the IDMC is as follows: A > C > B > D. Similarly, with the increase of the IP content, the 28 days flexural strength of the IDMC increases and then decreases. When the content of the IP is 20%, the pozzolanic activity and aggregate filling effect of the IP are fully developed. With the continuous increase of the IP content, the free water content in the samples decreases, the bond strength gradually reduces, and cracks occur in the samples prematurely, resulting in a lower flexural strength. In contrast, the B, C, and D have little influence. According to the analysis, the maximum 28 days flexural strength of the IDMC is obtained when the content of DA is 10%, SC is 1%, and mirabilite is 2%. The optimum mixing ratio for the sample to reach maximum flexural strength is $A_{K2}B_{K3}C_{K2}D_{K3}$.

3.4 Multi-index optimization analysis

Based on the results of the orthogonal tests, a multi-index optimization analysis is performed to optimize the indexes

Table 6: Three-layer structure model

Index	Initial setting time	28 days compressive strength		28 days flexural strength
Factor	A	B	C	D
Level	0, 20, 40%	0, 5, 10%	0, 1, 2%	0, 1, 2%

of the IDMC. According to the orthogonal test results of the IDMC initial setting time, 28 days compressive strength, and flexural strength, a three-layer structural model consisting of indexes, factors, and levels is established, as shown in Table 6. The influence weight of each factor level on the test results is calculated by this model, and then the optimal scheme of orthogonal test and the primary and secondary order of influencing factors are determined. In this study, m factors are assumed to be considered in the orthogonal tests, each factor has n levels, and the average value of the orthogonal test indexes at the jth level of factor A_i is K_{ij}.

If the test indexes are the smaller, the mechanical properties are better, then let $K_{ij} = 1/K_{ij}$, the matrix M is established. On the basis of the index layer, let $T_i = 1/\sum_{j=1}^{n} K_{ij}$, where $\sum_{j=1}^{n} K_{ij}$ is the sum of the arithmetic mean of the test results of each level of an index, then the factor matrix T is established. Set s_i as the range of A_i levels, let $S_i = s_i/\sum_{i=1}^{m} s_i$, the level matrix S is established. The weight matrix L = MTS is established, and the total weight matrix of multi-index evaluation is defined as the average of the each index weight, $L_a = \frac{1}{m} \cdot \sum_{i=1}^{m} L$. The level corresponding to the maximum value in each factor in the matrix L_a is the best level of the factor.

Let the index layer matrix of the initial setting time of the IDMC be M_1, the factor layer matrix be T_1, the horizontal layer matrix be S_1, and the weight matrix be L_1, as follows:

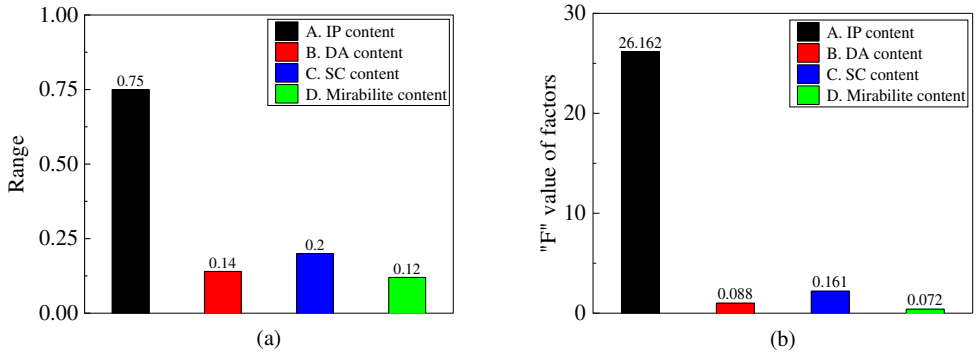

Figure 12: Range and variance analysis of 28 days flexural strength: (a) range analysis and (b) variance anlysis.

$$M_1 = \begin{bmatrix} \frac{1}{305.0} & \frac{1}{310.7} & \frac{1}{345.7} & 0 & 0 & 0 & 0 & 0 & 0 & 0 & 0 & 0 \\ 0 & 0 & 0 & \frac{1}{316.0} & \frac{1}{321.0} & \frac{1}{324.3} & 0 & 0 & 0 & 0 & 0 & 0 \\ 0 & 0 & 0 & 0 & 0 & 0 & \frac{1}{328.7} & \frac{1}{315.7} & \frac{1}{317.0} & 0 & 0 & 0 \\ 0 & 0 & 0 & 0 & 0 & 0 & 0 & 0 & 0 & \frac{1}{346.7} & \frac{1}{343.7} & \frac{1}{271.0} \end{bmatrix}^{\mathrm{T}}, \quad (1)$$

$$T_1 = \begin{bmatrix} 106.49 & 0 & 0 & 0 \\ 0 & 106.80 & 0 & 0 \\ 0 & 0 & 106.78 & 0 \\ 0 & 0 & 0 & 105.44 \end{bmatrix}, \quad (2)$$

$$S_1 = \begin{bmatrix} \frac{35}{132} & \frac{8.33}{132} & \frac{13}{132} & \frac{75.67}{132} \end{bmatrix}^{\mathrm{T}}, \quad (3)$$

$$L_1 = M_1 T_1 S_1 = [0.0926 \quad 0.0909 \quad 0.0817 \quad 0.0213 \quad 0.0210 \quad 0.0208 \quad 0.0320 \quad 0.0333 \quad 0.0332 \quad 0.1743 \quad 0.1759 \quad 0.2230]^{\mathrm{T}}. \quad (4)$$

Establishing the above similar matrix, M_2, T_2, and S_2 for 28 days compressive strength and M_3, T_3, and S_3 for 28 days flexural strength of the IDMC, and the weight matrices of the 28 days compressive strength and flexural strength of the IDMC are obtained as L_2 and L_3, as follows:

$$L_2 = M_2 T_2 S_2 = [0.2481 \quad 0.3077 \quad 0.1984 \quad 0.0207 \quad 0.0213 \quad 0.0215 \quad 0.0430 \quad 0.0460 \quad 0.0425 \quad 0.0167 \quad 0.0170 \quad 0.0172]^{\mathrm{T}}, \quad (5)$$

$$L_3 = M_3 T_3 S_3 = [0.1637 \quad 0.3048 \quad 0.1514 \quad 0.0364 \quad 0.0375 \quad 0.0418 \quad 0.0556 \quad 0.0600 \quad 0.0496 \quad 0.0304 \quad 0.0340 \quad 0.0347]^{\mathrm{T}}, \quad (6)$$

$$L_{\mathrm{a}} = \frac{L_1 + L_2 + L_3}{3} = [0.1681 \quad 0.2345 \quad 0.1438 \quad 0.0261 \quad 0.0266 \quad 0.0280 \quad 0.0435 \quad 0.0464 \quad 0.0418 \quad 0.0738 \quad 0.0756 \quad 0.0916]^{\mathrm{T}} = [A_{k1} \quad A_{k2} \quad A_{k3} \quad B_{k1} \quad B_{k2} \quad B_{k3} \quad C_{k1} \quad C_{k2} \quad C_{k3} \quad D_{k1} \quad D_{k2} \quad D_{k3}]^{\mathrm{T}}. \quad (7)$$

From the aforementioned matrix calculations, it is clear that the main order of the factors affecting the index values of the orthogonal tests is A > D > C > B. The factors A_{K2}, B_{K3}, C_{K2}, and D_{K3} have the greatest weights; thus, the optimal proportion of the IDMC is determined as $A_{K2}B_{K3}C_{K2}D_{K3}$. The contents of IP, DA, SC, mirabilite, and slag powder are 20, 10, 1, 2, and 67%, respectively. According to the proportions of the IDMC, the initial setting time is 270 min, and the 28 days compressive strength and flexural strength of the IDMC are 5.97 and 1.87 MPa, which meets the mine filling requirements.

4 Micro structure analysis of the IDMC

4.1 XRD analysis

Figure 13 shows the XRD diagram of the IDMC at different influencing levels. As shown in Figure 13(a), when the content of the IP is 20%, the intensity of characteristic peak of $Ca(OH)_2$ and AFt are the highest. The IP contains a lot of active SiO_2 and Al_2O_3. In the alkaline environment, $Ca(OH)_2$ reacts with the active material to produce C–S–H gels and AFt. According to the XRD semi-quantitative analysis, when the IP content is 20%, the mass fraction of SiO_2 in the matrix of the IDMC is the smallest. Compared with the sample with 40% content of the IP, the mass fraction of SiO_2 in the sample with 20% IP content is decreased by 5.8%, and the cementitious activity of the IP is fully stimulated.

As shown in Figure 13(b), as the DA content increases, the intensity of AFt characteristic peak gradually increases, and the intensity of $Ca(OH)_2$ characteristic peak gradually decreases. In the alkaline solution, the chemical bonds of Si–O and Al–O break to form Ca^{2+}, $[SiO_4]^{4-}$, and $[AlO_4]^{5-}$ ionic groups. $[SiO_4]^{4-}$ and $[AlO_4]^{5-}$ further hydrate to form C–S–H gels and hydrated calcium silicoaluminate. Meanwhile, the diffusion rate of SO_4^{2-} accelerates and it reacts with $Ca(OH)_2$ to generate AFt. According to the XRD semi-quantitative analysis, with the increase of the DA content, the mass fraction of SiO_2 in the matrix of the IDMC shows a downward trend. When the content of DA is 0, 5, and 10%, the mass fraction of SiO_2 is 80.3, 77.1, and 76.7%, respectively. As the DA content increases, the pozzolanic effect strengthens gradually, and the hydration degree of the IDMC is enhanced.

Figure 13(c) shows that with the increase in the SC content, the intensity of $CaCO_3$ and $Ca(OH)_2$ characteristic peaks increases gradually, and the intensity of the AFt characteristic peak increases and then decreases. The SC is easily soluble in water and hydrolyzes in the aqueous solution to produce HCO^{3-} and OH^-, increasing the PH

value of the solution. In the alkaline environment, the vitreous depolymerization of the IP and DA is accelerated, and AFt and C–S–H gels are further generated. Ca^{2+} generated during vitreous depolymerization reacts with CO_3^{2-} to form $CaCO_3$ precipitation, which increases the intensity of $CaCO_3$ characteristic peak. With the increase of SC, the $CaCO_3$ precipitation is adsorbed on the surface of the silica gels, slowing down the hydration reaction. Through the XRD semi-quantitative analysis, with the addition of the SC content, the mass fraction of SiO_2 in the matrix of the IDMC decreases and then increases. Compared with a 0% content of the SC, the mass fraction of SiO_2 decreases by 1.2% at 1% SC, and the cementitious activity of the IP and DA is fully stimulated at 1%.

According to Figure 13(d), with the increase of the mirabilite content, the intensity of the AFt characteristic peak gradually increases, and the intensity of $Ca(OH)_2$ characteristic peak gradually decreases. In the early stages of hydration, mirabilite can effectively improve the ionic strength in the liquid phase. SO_4^{2-} reacts with Ca^{2+}, Al^{3+}, and OH^- dissolved in the cementitious components to form AFt, which accelerates the setting and hardening of the IDMC. Through the XRD semi-quantitative analysis, as mirabilite content increases, the mass fraction of SiO_2 in the matrix of the IDMC shows a downward trend. When the content of the mirabilite is 0, 1, and 2%, the mass fraction of SiO_2 is 78.3, 75.6, and 74.0%, respectively. The hydration degree of the IP and DA is improved by increasing the mirabilite content.

4.2 SEM analysis

The micro morphology of the IDMC under different IP contents is shown in Figure 14. Compared with the 0% content of IP, the cementite matrix is mainly occupied by C–S–H gels, and the interface structure is denser when the IP content is 20%. When the content of IP is 40%, the slurry structure is relatively loose, the size of the interface hole is large and the distribution is uneven. The interfacial bond strength of the slurry is 20% > 0% > 40%.

Figure 15 depicts the micro morphology of the IDMC under different DA contents. When the content of DA is 0%, the interface structure is uneven, and the unhydrated slag particles are closely embedded in the hydration products. When the content of DA is 10%, the interface structure is relatively smooth without obvious protrusion, and a large amount of C–S–H gels and AFt are generated. The interfacial bond strength of the slurry is 10% > 5% > 0%.

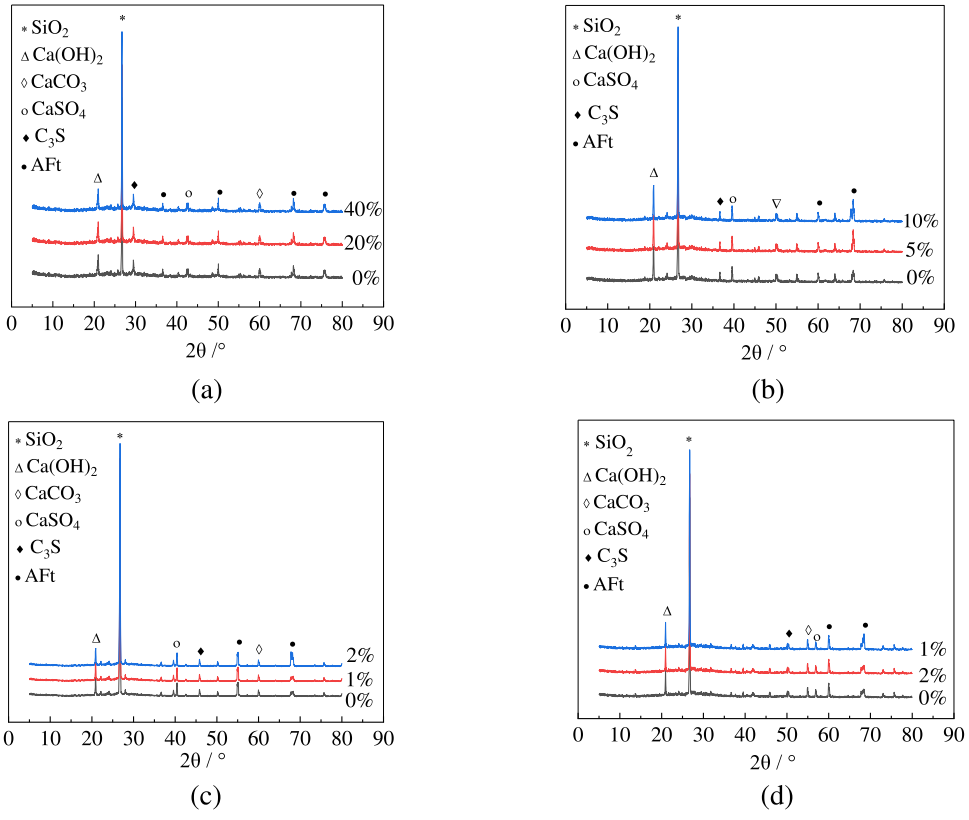

Figure 13: XRD analysis under the influence of various factors: (a) IP content, (b) DA content, (c) SC content, and (d) mirabilite content.

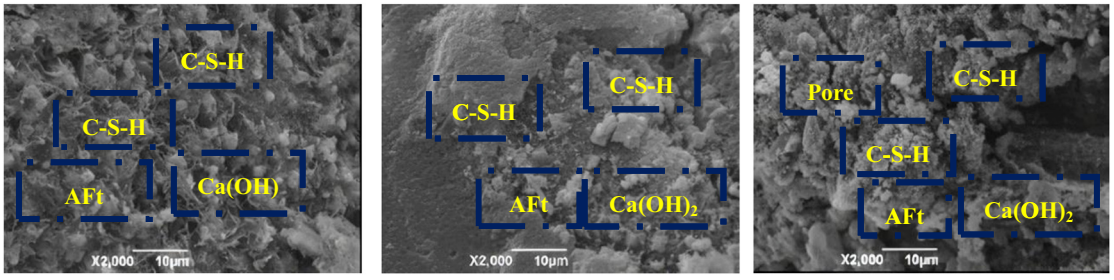

0% 20% 40%

Figure 14: SEM analysis of the IP content.

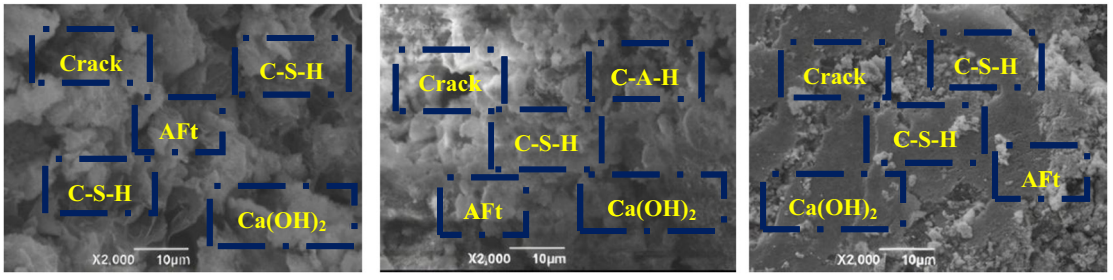

0% 5% 10%

Figure 15: SEM analysis of the DA content.

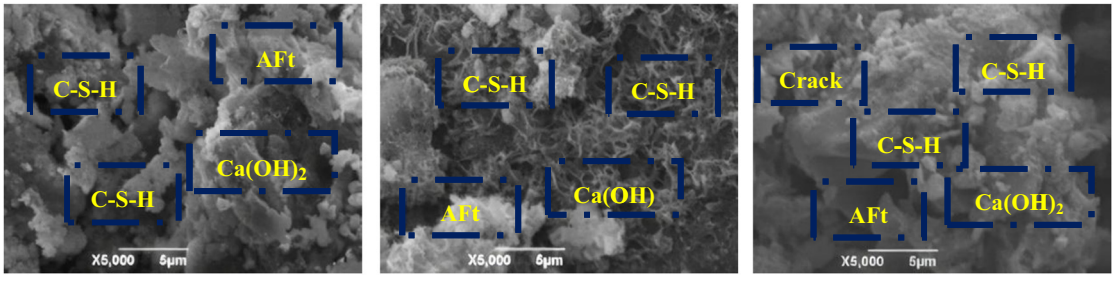

0% 1% 2%

Figure 16: SEM analysis of the SC content.

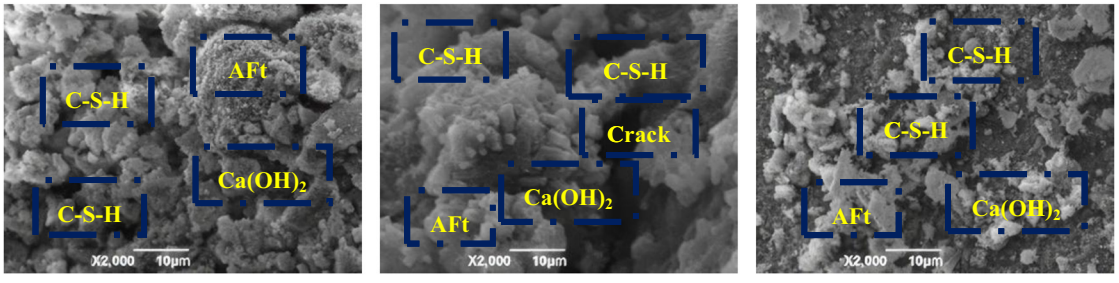

0% 1% 2%

Figure 17: SEM analysis of mirabilite content.

Figure 16 shows the micro morphology of the IDMC at various SC contents. When the content of SC is 0%, there are a large amount of non-hydrated cementitious components in the interface, fewer hydration products, and a quite loose interface structure. When the content of SC is 1%, a large amount of C–S–H gels and AFt are formed, and the interface structure is relatively tight. When the content of SC is 2%, the hydration products are relatively few, the crystal size of AFt is small, the interface structure is loose, and the number of pores is large. The interfacial bond strength of the slurry is 1% > 2% > 0%.

The micro morphology of the IDMC under different mirabilite contents is shown in Figure 17. When the content of mirabilite is 0%, C–S–H gels and columnar AFt are the main hydration products. The interface structure is dense, and no obvious cracks are observed. When the content of mirabilite is 1%, needle-like AFt is generated and filled in the pores between cementitious material particles. Meanwhile, a small amount of amorphous C–S–H gels on the surface of slag. When the content of mirabilite is 2%, a large amount of dense C–S–H gels are produced. Needle-like AFt crystals grow further in number and size, cross-filling larger pores and forming a compact mesh structure. The interfacial bond strength of the slurry is 1% > 2% > 0%.

5 Conclusions

This article presents the effects of IP content, DA content, SC content, and mirabilite content on mechanical properties and setting time of the IDMC. The micro morphology and phase composition of the hydration products are revealed. The following conclusions can be drawn.

1) The mirabilite content exerts the greatest influence on the initial setting time of the IDMC, and the addition of mirabilite can significantly reduce the initial time. As mirabilite content increases from 0 to 1% and 2%, the initial setting time of the IDMC is reduced by 0.87 and 21.83%, respectively. This is due to the fact that the increase of the mirabilite increases the hydration of IP and DA.
2) The IP content shows the greatest influence on 28 days compressive strength and flexural strength of the IDMC. With the increase of IP content, the 28 days compressive strength and flexural strength increase and then decrease. As the IP content increases from 0 to 20%, the compressive strength and flexural strength of the IDMC are increased by 24.01 and 86.25%, respectively. As the IP content increases from 20 to 40%, the compressive strength and flexural strength of IDMC are decreased by 35.53 and 50.34%, respectively.
3) According to the microscopic analysis, with the increase of the DA content, the pozzolanic effect is enhanced gradually, and the hydration degree of the IDMC is promoted. The SC hydrolyzes and generates HCO_3^- and OH^-, which provides an alkaline environment for the hydration reaction of the IDMC.
4) Based on multi-index optimization analysis, the optimum mix proportion of the IDMC is determined as the content of IP is 20%, DA is 10%, SC is 1%, mirabilite is 2%, and slag powder is 67%.

Acknowledgements: The authors wish to acknowledge the contribution of the National Natural Science Foundation of China and Anhui University of Technology.

Funding information: This study was sponsored by the Key Research and Development Project of Anhui Province (No. 2022i01020005), Major Science and Technology Project of Anhui Province (No. 202203a07020005), National Natural Science Foundation of China (No. 52078001), The University Outstanding Research and Innovation Team Program of Anhui Province (No. 2023AH010017), The University Synergy Innovation Program of Anhui Province (Nos. GXXT-2023-061 and GXXT-2022-074), and Wuhu Technology and Innovation Research Institute, Anhui University of Technology (No. 2022jc04).

Author contributions: All authors have accepted responsibility for the entire content of this manuscript and consented to its submission to the journal, reviewed all the results and approved the final version of the manuscript. FY: supervision, writing – review and editing, and funding acquisition. XC: writing – original draft and validation. YC: formal analysis and data curation. YF: methodology, writing – review and editing, and project administration. SB: investigation and formal analysis. SZ: validation and investigation.

Conflict of interest: Authors state no conflict of interest.

Data availability statement: The datasets generated during and/or analysed during the current study are available from the corresponding author on reasonable request.

References

[1] United States Geological Survey-USGS-USGS. Mineral commodity summaries. Iron Ore; 2020. https://pubs.usgs.gov/periodicals/mcs2020/mcs2020-iron-ore.pdf.

[2] Fang D, Liao X, Zhang X, Teng A, Xue X. A novel resource utilization of the calcium-based semi-dry flue gas desulfurization ash: As a reductant to remove chromium and vanadium from vanadium industrial wastewater. J Hazard Mater. 2017;342(15):436–45. doi: 10.1016/j.jhazmat.2017.08.060.
[3] Ma K, Deng J, Ma P, Sun C, Zhou Q, Xu J. A novel plant-internal route of recycling sulfur from the flue gas desulfurization (FGD) ash through sintering process: From lab-scale principles to industrial practices. J Environ Chem Eng. 2022;10(1):106957. doi: 10.1016/j.jece.2021.106957.
[4] Zhou D, Wei R, Zhu Y, Wang Y, Huang B, Long H, et al. Calcium sulfate whisker one-step preparation using semi-dry flue gas desulfurization ash and directional growth control. J Clean Prod. 2021;290(25):125754. doi: 10.1016/j.jclepro.2020.125754.
[5] Jawad A, Fadi A, Awad M, Farouk D, Onuralp Ö, Cut R. Durability and microstructure analysis of concrete made with volcanic ash: A review (Part II). Sci Eng Compos Mater. 2023;30(1):2022021. doi: 10.1515/SECM-2022-0211.
[6] Gou M, Zhou L, Then N. Utilization of tailings in cement and concrete: A review. Sci Eng Compos Mater. 2019;26(1):449–64. doi: 10.1515/secm-2019-0029.
[7] Shi J, Pan W, Kang J, Yu Z, Sun G, Li J, et al. Properties of Ultra-High Performance concrete incorporating iron tailings powder and iron tailings sand. J Build Eng. 2024;83(15):108442. doi: 10.1016/j.jobe.2024.108442.
[8] Chen F, Zhang L, Zou C, Zhu X, Fang Q, Xu S. Study on influencing factors of shear characteristics of rock-fill concrete layer of iron tailings as fine aggregate. Constr Build Mater. 2022;345(22):128213. doi: 10.1016/j.conbuildmat.2022.128213.
[9] Chen J, Yuan Y, Zhu Q, Duan J. High-temperature resistance of high-strength concrete with iron tailing sand. J Build Eng. 2023;63(PA):105544. doi: 10.1016/j.jobe.2022.105544.
[10] Shettima A, Hussin M, Ahmad Y, Mirza J. Evaluation of iron ore tailings as replacement for fine aggregate in concrete. Constr Build Mater. 2016;120(1):72–9. doi: 10.1016/j.conbuildmat.2016.05.095.
[11] Han F, Song S, Liu J, Huang S. Properties of steam-cured precast concrete containing iron tailing powder. Powder Technol. 2019;345:292–9. doi: 10.1016/j.powtec.2019.01.007.
[12] Liu K, Wang S, Quan X, Jing W, Xu J, Zhao N, et al. Effect of iron ore tailings industrial by-product as eco-friendly aggregate on mechanical properties, pore structure, and sulfate attack and dry-wet cycles resistance of concrete. Case Stud Constr Mater. 2022;17:e01472. doi: 10.1016/j.cscm.2022.e01472.
[13] Kong L, Xie S, Wang C, Wang L. Effect of iron tailings as fine aggregate and mineral admixture on strength and microstructure of cement mortar. Int J Concr Struct Mater. 2023;17(1):24. doi: 10.1186/s40069-023-00584-6.
[14] Silva B, Henrique M, Souza M, Paulino T, Silva C, Brigolini J, et al. Study of mechanical, durability and microstructural properties of cementitious composite with addition of different iron ore tailings from Brazil. J Mater Res Technol. 2022;18:1947–62. doi: 10.1016/j.jmrt.2022.03.070.
[15] Yao G, Wang Q, Wang Z, Wang J, Lyu X. Activation of hydration properties of iron ore tailings and their application as supplementary cementitious materials in cement. Powder Technol. 2020;360:863–71. doi: 10.1016/j.powtec.2019.11.002.
[16] Cheng Y, Yang S, Zhang J, Sun X. Test research on hydration process of cement-iron tailings powder composite cementitious materials. Powder Technol. 2022;399:117215. doi: 10.1016/j.powtec.2022.117215.
[17] Luo T, Yi Y, Liu F, Sun Q, Pan X, Hua C. Early-age hydration and strength formation mechanism of composite concrete using molybdenum tailings. Case Stud Constr Mater. 2022;16:e01101. doi: 10.1016/j.cscm.2022.e01101.
[18] Deng D, Liu L, Yao Z, Song K, Lao D. A practice of ultra-fine tailings disposal as filling material in a gold mine. J Environ Manag. 2017;196(1):100–9. doi: 10.1016/j.jenvman.2017.02.056.
[19] Lu H, Qi C, Chen Q, Gan D, Xue Z, Hu Y. A new procedure for recycling waste tailings as cemented paste backfill to underground stopes and open pits. J Clean Prod. 2018;188(1):601–12. doi: 10.1016/j.jclepro.2018.04.041.
[20] Chu C, Deng Y, Zhou A, Feng Q, Ye H, Zha F. Backfilling performance of mixtures of dredged river sediment and iron tailing slag stabilized by calcium carbide slag in mine goaf. Constr Build Mater. 2018;189(20):849–56. doi: 10.1016/j.conbuildmat.2018.09.049.
[21] Li B, Xiao L, Fu Y. Activity evaluation of a tailing in a cementitious system. Key Eng Mater. 2017;726:515–20. doi: 10.4028/www.scientific.net/KEM.726.515.
[22] An S, Liu J, Cheng L, Guo L, Zhou D. Rheological and mechanical properties of full-tailings backfill material prepared by ultrafine-iron-tailings-powder-based consolidation agent. Constr Build Mater. 2024;417(23):135286. doi: 10.1016/j.conbuildmat.2024.135286.
[23] Duan S, Liao H, Cheng F, Song H, Yang H. Investigation into the synergistic effects in hydrated gelling systems containing fly ash, desulfurization gypsum and steel slag. Constr Build Mater. 2018;187(30):113–1120. doi: 10.1016/j.conbuildmat.2018.07.241.
[24] Jiang L, Li C, Wang C, Xu N, Chu H. Utilization of flue gas desulfurization gypsum as an activation agent for high-volume slag concrete. J Clean Prod. 2018;205(20):589–98. doi: 10.1016/j.jclepro.2018.09.145.
[25] Duan S, Liao H, Cheng F, Tao M. Effect of curing condition and carbonization enhancement on mechanical properties of fly ash-desulfurization gypsum-steel slag blocks. J CO2 Utilization. 2020;38:282–90. doi: 10.1016/j.jcou.2020.02.004.
[26] Xu Z, Hu D, An R, Lin L, Xiang Y, Han L, et al. Preparation of superfine and semi-hydrated flue gas desulfurization gypsum powder by a superheated steam powdered jet mill and its application to produce cement pastes. Case Stud Constr Mater. 2022;17:e01549. doi: 10.1016/j.cscm.2022.e01549.
[27] Vashistha P, Park S, Pyo S. A review on sustainable fabrication of futuristic cementitious binders based on application of waste concrete powder, steel slags, and coal bottom ash. Int J Concr Struct Mater. 2022;16(1):51. doi: 10.1186/s40069-022-0054-9.
[28] Li X, Chen Q, Ma B, Huang J, Jian S, Wu B. Utilization of modified CFBC desulfurization ash as an admixture in blended cements: Physico-mechanical and hydration characteristics. Fuel. 2012;102:674–80. doi: 10.1016/j.fuel.2012.07.010.
[29] Wang C, Tan K, Xu X, Wang P. Effect of Activators, Admixtures and temperature on the early hydration performance of desulfurization ash. Constr Build Mater. 2014;70(15):322–31. doi: 10.1016/j.conbuildmat.2014.07.095.
[30] Guo L, Wang H, Zhong L, Zhang J, Lu L. Preparation and characterization of titanium gypsum artificial aggregate. Sci Eng Compos Mater. 2024;31(1):20240004. doi: 10.1515/SECM-2024-0004.
[31] Ignazio B, Antonio D, Veronica V, Luigi V, Michelina C. Metakaolin-based geopolymers filled with volcanic fly ashes: FT-IR, thermal characterization, and antibacterial property. Sci Eng Compos Mater. 2023;30(1):20220192. doi: 10.1515/SECM-2022-0192.

[32] Sun R, Wang D, Fang Z, Wu Y, Zhuang S, Kang L, et al. Study on the steel slag-desulfurized ash based solid waste cementitious materials and its mortars interface transition zone. Met Mine. 2022;547:41–52. doi: 10.19614/j.cnki.jsks.202201006.
[33] Zhang S, Zhao T, Li Y, Li Z, Li H, Zhang B, et al. The effects and solidification characteristics of municipal solid waste incineration fly ash-slag-tailing based backfill blocks in underground mine condition. Constr Build Mater. 2024;420(22):135508. doi: 10.1016/j.conbuildmat.2024.135508.
[34] Frasson B, Rocha J. Drying shrinkage behavior of geopolymer mortar based on kaolinitic coal gangue. Case Stud Constr Mater. 2023;18:e01957. doi: 10.1016/j.cscm.2023.e01957.
[35] GB/T 1346-2011. Test methods for water requirement of normal consistency, setting time and soundness of the Portland cement. Beijing, China: National Standards of People's Republic of China; 2011.
[36] GB/T 17671-2021. Test method of cement mortar strength(ISO method). Method of testing cements-Determination of strength. Beijing, China: National Standards of People's Republic of China; 2021.